Research Article

Lightweight design and integrated method for manufacturing hydraulic wheel-legged robots

Xu LI[1,2✉], Haoyang YU[1], Huaizhi ZONG[2], Haibo FENG[1] and Yili FU[1✉]

[1]State Key Laboratory of Robotics and System, Harbin Institute of Technology, Harbin 150001, China
[2]State Key Laboratory of Fluid Power and Mechatronic Systems, Zhejiang University, Hangzhou 310027, China

Abstract: Design and manufacturing play pivotal roles in hydraulic-driven robotic development. However, previous studies have emphasized mainly results and performance, often overlooking the specifics of the design and manufacturing process. This paper introduces a novel approach known as lightweight design and integrated manufacturing (LD&IM) for hydraulic wheel-legged robots. The LD&IM method leverages topology optimization and generative design techniques to achieve a substantial 45% weight reduction, enhancing the robot's dynamic motion capabilities. This innovative design method not only streamlines the design process but also upholds the crucial attributes of lightweight construction and high strength essential for hydraulic wheel-legged robots. Furthermore, the integrated manufacturing method, incorporating selective laser melting (SLM) and high-precision subtractive manufacturing (SM) processes, expedites the fabrication of high-quality components. Using the LD&IM approach, a hydraulic-driven single wheel-legged robot, denoted WLR-IV, has been successfully developed. This robot boasts low mass and inertia, high strength, and a simplified component structure. To assess its dynamic jumping capabilities, the control loop integrates a linear quadratic regulator (LQR) and zero dynamic-based controller, while trajectory planning uses the spring-loaded inverted pendulum (SLIP) model. Experimental jumping results confirm the WLR-IV single-legged robot's exceptional dynamic performance, validating both the effectiveness of the LD&IM method and the rationale behind the control strategy.

Key words: Wheel-legged robot, Hydraulic driven, Topology optimization, Additive manufacturing, Jump Control

1 Introduction

1.1 Background

The transition from Industry 4.0 to Industry 5.0 production systems is poised to have a profound impact on the manufacturing landscape. In the context of Industry 4.0, the pivotal role of human-machine collaboration and advanced artificial intelligence (AI) technologies is paramount in augmenting the industry's adaptability and sustainability (Majern k, 2022). Nevertheless, the training and upskilling of experienced engineers require a substantial investment in terms of cost and time, and there may be challenges associated with resistance from incumbent employees.

In contrast, Industry 5.0 places a heightened emphasis on the enhancement of collaboration between humans and robots (Maddikunta, 2022), with the primary objective of bolstering manufacturing flexibility. This collaborative paradigm effectively harnesses human ingenuity, problem-solving abilities, and adaptability, and seamlessly integrates them with the precision, speed, and reliability of robotic systems. This synergistic approach is expected to substantially augment the industry's capacity to handle intricate tasks, thereby affording human workers the opportunity to concentrate their efforts on assignments that demand judgment, decision-making prowess, and fine motor skills.

In the context of the development of biomimetic legged robots, the collaborative synergy between human engineers and computational resources represents a pivotal avenue for augmenting development efficiency. This cooperative approach allows human engineers to judiciously allocate their attention to-

✉ Xu LI, hitlx@hit.edu.cn
  Yili FU, meylfu@hit.edu.cn
  Xu LI, https://orcid.org/0000-0003-1898-9948

wards the refinement of a robot's functional and performance attributes. More specifically, the intricacies of structural design, encompassing considerations such as lightweight construction and strength validation, can be effectively delegated to computer-based systems. This delegation liberates valuable human resources within the domain of robot development, empowering designers to channel their energies toward the enhancement of the robot's overall performance and capabilities. The mutually beneficial fusion of human expertise and computational assistance represents a promising pathway for advancing the field of biomimetic legged robot design and engineering.

The development of biomimetic legged robots entails the integration of diverse technologies to address multifaceted tasks. A critical aspect of this endeavor involves ensuring the seamless coordination of various hardware and software components. The incorporation of advanced technologies, such as intricate mechanism design and efficient material utilization, into existing manufacturing processes not only adds complexity but also necessitates rapid implementation. These challenges underscore the inherent difficulties in smoothly integrating new technologies into the established paradigm of robot production. Previous research efforts have concentrated mainly on enhancing manufacturing methods or investigating materials for specific robot components, often neglecting an holistic approach to designing and manufacturing robot elements. In this study we sought to fill this research gap by introducing a novel methodology termed "lightweight design and integrated manufacturing (LD&IM)" for hydraulic wheel-legged robots. LD&IM promises to enhance the efficiency and cost-effectiveness of robot development, addressing these complex challenges.

1.2 Robotics

The 2015 DARPA robotics challenge results affirmed the efficient mobility achieved through the combination of wheels and legs (Karumanchi et al., 2017). Wheels excel on flat terrain, while legs adapt to various complex terrains (Bae et al., 2016, Stentz et al., 2015; DeDonato et al., 2017, Knabe et al., 2018, Tsagarakis et al., 2017). Scenarios like field detection, interstellar exploration, and rescue operations neces-

sitate robots with a strong load-carrying capacity. Hydraulic-driven robots, characterized by a high power-to-weight ratio and remarkable impact resistance (Hyon et al., 2016), provide effective solutions. Atlas, a highly dynamic hydraulic humanoid robot, effectively uses topology optimization and generative design, integrating the hydraulic system with its skeleton to enhance heat dissipation. This application of topology optimization techniques has been extended to motor-driven quadruped robots (Sun et al., 2023) and biped wheel-legged robots (Klemm et al., 2019). The goal is to create lighter structures conducive to more dynamic and agile movements. Specifically, designing a hydraulic-driven wheel-legged robot requires light weight, high-strength, and multifunctional integration to facilitate dynamic maneuvers, such as overcoming obstacles.

The design process is inherently complex, with a multitude of factors to consider. Many design requirements are subjective and abstract, rendering the establishment of a parametric design process challenging (Kien and Zhuang, 2021). While factors like part load and size can be parameterized, aspects such as ensuring smooth operation, manufacturability, and aesthetic appeal defy straightforward parametric representation. These elements are often subjective and heavily reliant on the designer's creativity. To address intricate design challenges marked by incalculable performance criteria, a practical generative CAD-based design exploration approach is recommended (Krish, 2011). A mathematical model introduced later (Glowinski et al., 2020) facilitates a rational linkage between the hydraulic driving unit and the exoskeleton structure.

1.3 AM/Topology Optimization

The unique contribution of our study is the introduction of a comprehensive design approach that amalgamates additive manufacturing (AM) and topology optimization (Liu et al., 2018, Großmann et al., 2020) for wheel-legged robots. The introduced lightweight design method unlocks new possibilities for crafting highly integrated and lightweight structures, such as the innovative design and manufacturing strategies used in the creation of the WLR-IV single-legged robot (Fig. 1). These approaches col-

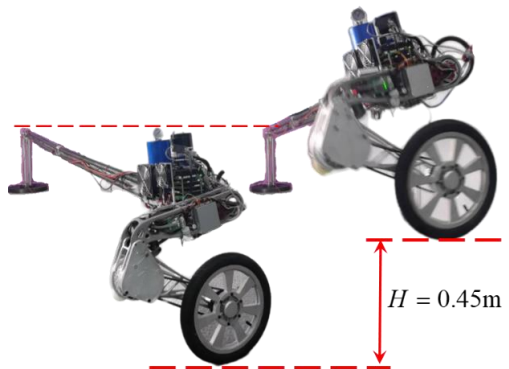lectively result in a lighter and stronger robotic design.

Fig. 1 WLR-IV Single-Legged Robot

Once the design phase concludes, efficient part manufacturing becomes a paramount challenge. Additive manufacturing (AM) or 3D printing offers distinct advantages, including design flexibility, waste reduction, and the capability to produce intricate structures swiftly (Ngo et al., 2018). The fusion of generative design and AM flexibility (Zhang et al., 2021) is being increasingly harnessed for producing high-performance functional structures and digital materials across various domains (Wu et al., 2019).

Unlike traditional subtractive manufacturing, layer-based AM, such as selective laser melting (SLM), excels in crafting intricate parts (Emmelmann et al., 2013). SLM, used in manufacturing hydraulic components (Yap et al., 2015), uses a high-power-density laser to melt and fuse metallic powders, yielding parts with excellent mechanical properties that align with the stringent demands of hydraulic components, ensuring crack-free, high-strength characteristics.

While steel and titanium are frequently used in SLM, the high density of steel does not align with the stringent weight requirements of a wheel-legged robot's structure. Titanium and its alloys present challenges in conventional processes due to their sensitivity to oxygen, nitrogen, hydrogen, and carbon, hindering precision machining methods like finish turning, grinding, and polishing (Herzog et al., 2016). As for AM, only a few Al alloys are currently used, offering easier post-processing and cost-efficiency compared to Ti alloys (Brice et al., 2015).

Furthermore, high thermal conductivity in aluminum alloys reduces internal thermal stresses and aids heat dissipation in hydraulic systems. In our research, the chosen high-strength aluminum alloy (AlMg-ScZr) boasts a yield strength of 480-550 MPa and a density of 2.66 g/cm³. These attributes meet the wheel-legged robot's prerequisites of light weight and high strength while mirroring the thermal conductivity and process attributes of forged aluminum alloy 7075-T6 (Martin et al., 2017).

In this paper, we introduce a lightweight and high strength generative design method (Section 2) for hydraulic wheel-legged robots. To bridge the gap between concepts and real parts, we propose a manufacturing approach that combines precision machining with AM (Section 3). We enhance flow channel quality using fluid polishing technology. We assess structure and system reliability (Section 4) with a jump control method based on LQR (Section 5). Section 6 details experimental setups and outcomes for HDU displacement/force tracking and jump experiments. Our work presents an innovative design and manufacturing method to meet high strength and light weight demands through combined additive and subtractive manufacturing. Conclusions and prospects are listed in Section 7.

2 Lightweight design method

A crucial objective in designing hydraulic robot parts is achieving both high strength and light weight characteristics. While various methods to approach this goal have been explored by researchers (Semini et al., 2016, Raibert et al., 2008; Rong et al., 2012), a clear design concept and process flow for hydraulic robot parts remains lacking. In this section, a reliable and efficient lightweight design method for hydraulic robots and the corresponding processing technology are proposed in the field of hydraulic robot part design.

2.1 Design objectives

The key characteristics of wheel-legged robots are their maneuverability on flat ground and strong adaptability on complex terrain, especially their jumping ability when encountering obstacles. The main aims of the design of high dynamic wheel-legged robots are:

1) Light weight and low inertia

2) Excellent impact resistance

3) Minimal use of printing powder

4) Convenience in the subtractive manufacturing process

5) Low flow resistance in hydraulic pipelines

Items 1 and 2 are key objectives in mobile robot design. Prioritizing light weight and low inertia enhances a robot's motion performance for the same driving power. Item 3 focuses mainly on cost-saving during manufacturing. While 3D printing can create conceptual models, it is essential to consider material requirements for the subtractive manufacturing process. Design must account for clamping, positioning, and measurement procedures. Item 5 streamlines part production, emphasizing a smooth hydraulic flow pipeline design to reduce resistance. Aesthetics also matter in part appearance, and innovative design ideas coupled with advanced computing technologies elevate the visual appeal. This design approach not only meets these goals but also suits complex multi-criteria design challenges with unquantifiable performance criteria.

2.2 Design process

Design is an iterative and co-evolutionary process of searching the design space and the solution space (Maher and Poon, 1996). The flow chart of the design method for the hydraulic wheel-legged robot is divided into three steps (Fig. 2).

The initial step of this process entails function design, where we meticulously outline the form and dimensions of the components in alignment with the overarching robot structure. Furthermore, we design the actuator in accordance with the load-bearing capabilities and motion specifications commensurate with the component's size. Subsequently, the transmission mechanism is methodically developed to accommodate the articulated motion requisites. Typically, motor-driven transmissions include harmonic reducers, planetary reducers, and synchronous belts, while hydraulic-driven transmissions often involve direct drive or connecting rod mechanisms. This phase culminates in the attainment of the part's fundamental functionality, meeting the essential prerequisites for installation and power transmission.

The second step, generative design, represents a pivotal stage in the realization of lightweight and high strength components. Precise load calculations and the delineation of a design domain are crucial facets of part design, exerting a profound influence on both the overall aesthetics and structural robustness of the component. The delineation of the design domain, contingent on the installation site and the part's range of motion, demands a conscientious allowance for internal moving components such as pistons and
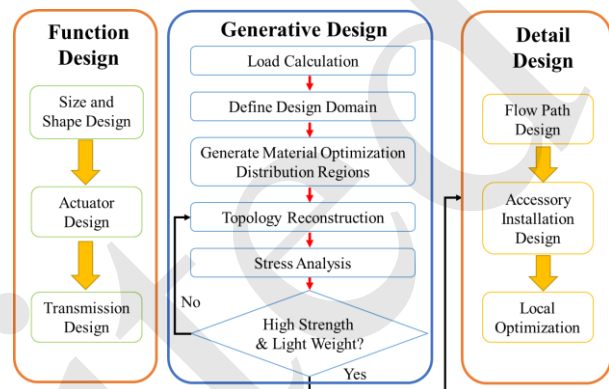

Fig. 2 Lightweight design method for hydraulic wheel-legged robot

connecting rods. Notably, in load calculations, it is imperative to account not only for static forces but also dynamic impact forces. Leveraging these load specifications and the defined design domain, advanced computational tools such as Inspire are harnessed to automatically generate material optimization distribution regions. These regions, characterized by subsets of the design domain that meet the requisite load criteria, provide the foundation for subsequent topological optimization, which fundamentally reshapes the mechanical structure of the components. The objective of topology optimization in this work is to distribute the material in a certain region in the most favorable way to minimize the mass of the part while satisfying the stress and mounting dimensional constraints. The specific optimization problem and objectives are shown in the electronic supplementary materials (ESM).

Function design serves as the foundation for generative design. It provides the necessary functional specifications and structural requirements, and determines the boundaries and constraints for generative design. The material growth produced by generative design must conform to the predefined func-

tional aspects outlined in the function design phase, ensuring that the final design does not interfere with the intended function of the part.

Finally, we enter the third step, detail design. The most important step in the detail design of hydraulic parts is the optimization of the flow channel, which requires increasing the mass as little as possible without affecting the stress conditions of parts. In addition, the design of the flow channel should be as smooth as possible to reduce flow resistance. Finally, the installation hole and surface of accessory parts are designed and optimized locally.

2.3 Examples of Lightweight Design Methods

The following is an example of thigh design in which details of the design process are described. The thigh connects the knee and hip joint, including the actuators and transmission mechanism of the hip pitch and knee joints. First, from previous design experience, the appropriate length is 350 mm, and the width and height are each 80 mm. In terms of actuator design, because the linear cylinder and thigh have a prismatic shape, their axes are approximately parallel to save space and improve structural compactness. Then based on the joint loads (about 250 Nm) and the standard size of the cylinder, we designed the size of the hip and knee cylinder (cylinder diameter: 20 mm, rod diameter: 12 mm). The transmission design considers two main factors: one is how to convert the linear motion of the cylinder into the rotation of the joint approximately linearly and to cover the range of the robot's motion angle. The other is the relationship between the moment arm length and the angle in the transmission process.
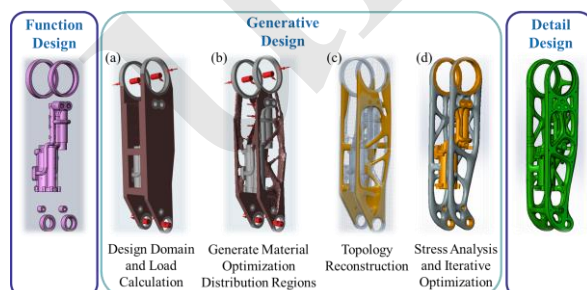

Fig. 3 The design process of the HIT WLR-IV thigh

Then we enter the second step: generative design. The function design determines the position of the hydraulic cylinder and the positions for installa-

tion of the linear guide rail, connecting rod and bearing. There remain some scattered entities, as shown on the left in Fig. 3. It is very difficult to connect these scattered entities into an integral part. The generative design method can solve this problem quickly and effectively. Firstly, we need to define the design domain (Fig. 3a), that is, the area where materials can be arranged to connect the scattered entities from the function design. Then calculate the load. The thigh not only bears the gravity of the robot itself but also needs to resist the landing impact force when the robot jumps, which is taken as the maximum load condition. The cylinder bears the peak pressure (21 Mpa). The base of the guide rail mounting bears the force (about 600 N) from the guide rail, and the pin shaft connecting hole also bears part of the impact force. Then the model is imported into Inspire software to automatically calculate the material optimization distribution regions (Fig. 3b). Next, the connection part is reconstructed based on topology optimization (Fig. 3c). The parts designed in this way should be the lightest, in theory. Finally, repeated finite element analysis (Fig. 3d) was carried out on the thigh part model, and the structure was optimized to ensure the reliability of the thigh structure and at the same time pursue the design goal of light weight.

After repeated finite element analysis of the thigh parts, the result is shown in Fig. 4. Under the ultimate load of 1000 kg jump impact, the stress analysis results (Fig. 4a) show that the maximum stress is 241.2 Mpa, and the strain analysis results (Fig. 4b) show that the maximum strain is 0.677 mm. The meta-analysis results are all within the safe region of the material, and the maximum strain is negligible compared to the motion range of the robot. Through repeated finite element analysis and structural optimization of the designed parts, the structural reliability of the parts under the worst working conditions during robot motion is guaranteed.

The third step: detailed design. Optimizing the hydraulic pipeline based on the topological structure of low flow resistance can save as much material as possible. The thigh also needs to install an LVDT, pressure sensor, driver and other accessories. We need to design the corresponding installation hole. Finally, appearance and other details are optimized.
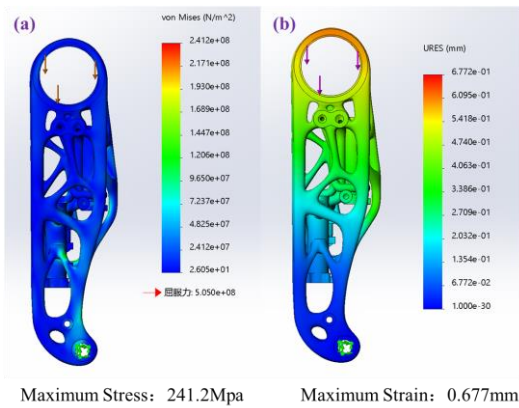
Maximum Stress：241.2Mpa   Maximum Strain：0.677mm

Fig. 4 Finite element analysis results of the thigh part

The optimized thigh is shown in Fig. 5c. Compared with an integrated thigh (Fig. 5b) produced by the subtractive manufacturing process (Li et al., 2019), the weight of the WLR-IV thigh is reduced by more than 50%. Compared with the first generation of the fabricated thigh as shown in Fig. 5a (Li et al., 2018), the number of components required is reduced from 20 to 1.
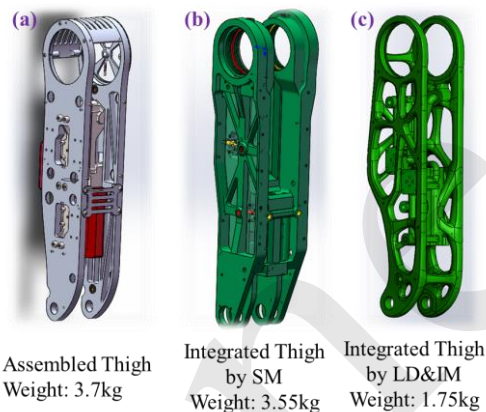

Assembled Thigh
Weight: 3.7kg

Integrated Thigh
by SM
Weight: 3.55kg

Integrated Thigh
by LD&IM
Weight: 1.75kg

Fig. 5 Evolution of the thigh design for WLR series robots.
(a) The assembled thigh for WLR-I. (b) The integrated
thigh produced by SM for WLR-II. (c) The integrated
thigh produced by LD&IM for WLR-IV

The same design method was used for the calf design. The final structure is shown in Fig. 6. The weight of the calf is reduced by 35% compared with that made by SM. According to the results of the WLR-IV single-legged robot structure design, the weight of parts can be greatly reduced using the design method proposed in this paper.

Calf by SM
Weight: 1460g

Calf by LD&IM
Weight: 946g

Fig. 6 More than a 35% reduction in calf weight was achieved using the LD&IM method

2.4 Design implementation

The comprehensive design process discussed above necessitates the use of multiple CAD/CAE design software tools. Each of these software tools, along with their respective functions, is delineated in Fig. 7. Initially, SolidWorks was used for functional design, using modeling commands like stretching and scanning. Subsequently, Inspire was used to configure the part's design domain, set material properties, elastic modulus, and establish simulation parameters including loading, boundary conditions, constraints, and solver options. These parameters have a direct influence over the precision and dependability of simulation outcomes. Inspire software is also instrumental in simulating the optimal material distribution within the part.

Leveraging the versatile modeling capabilities of Evolve, in this study we conducted topological reconstruction of areas of optimal material distribution, enhancing the regularity and aesthetics of the component's shape. Notably, while the optimized topology is predicated on the material distribution obtained through simulation calculations, it is subjected to validation through professional stress simulation software, ANSYS, to ensure enhanced safety and reliability. Through iterative optimization processes, UG software is subsequently used to incorporate finer features such as screw holes and rounded edges. The design process culminates by returning to SolidWorks for component assembly and the generation of 2D drawings. At this juncture, the specific design and
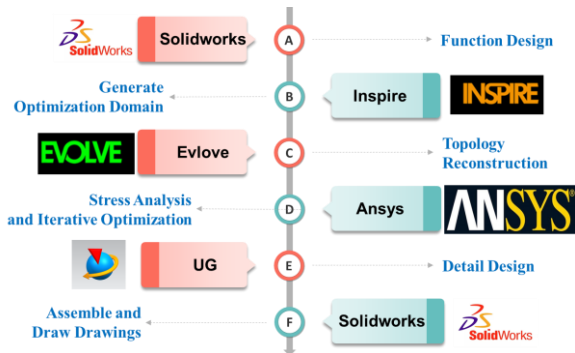
implementation of the components are deemed complete.

Fig. 7 Software used in the design process

3 Integrated Manufacturing

The optimized model designed in section II is a 3D model containing a very complex irregular surface and internal curved pipeline. It is difficult or even impossible to produce such complex models using conventional manufacturing technologies. A set of complex and reasonable manufacturing methods is needed to bridge the gap between the conceptual model and practical parts.
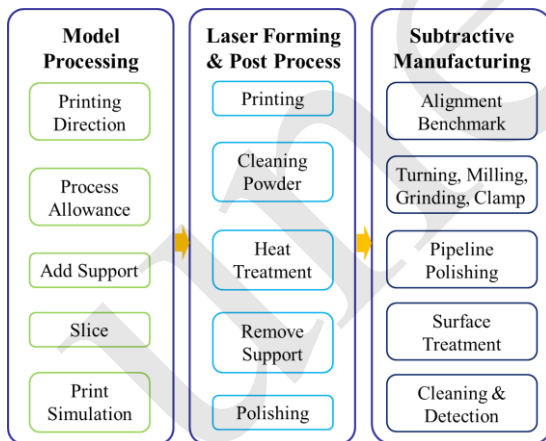
3.1 Manufacturing process

Fig. 8 Integrated manufacturing method of hydraulic robot parts

As shown in Fig. 8, the integrated manufacturing method proposed is divided into three main steps: model processing, laser forming and post-processing, and reduction manufacturing. In the process of model processing, it is important to plan the optimum printing orientation of the part. The principle to follow is to reduce the amount of powder and ensure the molding quality of the key surface. Then a process allowance (generally 0.5-2.0 mm) is added to ensure the amount of machine grinding and cutting. A surface with good forming quality can require less machining allowance. After that, the supporting materials are added, which must support the growth of subsequent layers and can be easily removed after printing. The final process is to slice the part into sufficient thin layers and simulate the printing process to expose possible forming problems as early as possible. After model processing, the model is printed automatically in the metal additive manufacturing system BLT S600. The SLM has the advantage of using unbound powder, which can easily be removed by air pressure after printing. Heat treatment is used to eliminate residual stress and improve fatigue resistance. The supporting structure is removed and the surface of the parts is polished, which is usually done manually by workers.

Subtractive manufacturing aims mainly at the precision machining of the surface and hole that needs to be assembled and matched with other parts. The benchmark surface of parts should be considered in the design of process allowance, to facilitate the subsequent conventional processes such as turning, milling, grinding and clamping. The internal hydraulic pipeline of the part cannot be polished by the traditional grinding method. To reduce flow resistance, the abrasive flow polishing process used in this work can solve the problem of a rough pipeline of printing parts. The result of abrasive flow polishing is shown in Fig. 9. The internal pipeline has poor roughness due to the lack of support materials (Semini et al., 2015). Generally, the original roughness is between Ra 12 and Ra 32, which can reach Ra 6.3 after rough polishing and Ra 1.6-3.2 after fine polishing. Surface treatment includes sulfuric acid oxidation to obtain the specified color or hard anodizing to obtain a wear-resistant surface. Finally, cleaning and dimensional error detection are completed to obtain high quality parts.

Fig. 9 Comparison of results from abrasive flow polishing

3.2 Manufacturing implementation

The production of intricate hydraulic components necessitates an array of specialized equipment (Fig. 10). In this study, in which the robot was constructed from large, high-strength aluminum materials, BLT-S600 series equipment was selected as the prime choice. Following this, wire cutting equipment is used to separate the printed parts from the printing substrate, with subsequent manual polishing and related processes to eliminate printing support and refine the parts' surfaces. These components are then securely affixed to the appropriate fixtures for CNC milling of the assembly surfaces. To cater to parts demanding precision machining, such as hydraulic cylinders and oil joints, equipment like grinders and mirror EDM is used to ensure high-quality machining. Lastly, hydraulic pipeline polishing is accomplished mainly using abrasive flow polishing equipment, facilitating the precise polishing of curved flow channels through abrasive compression.
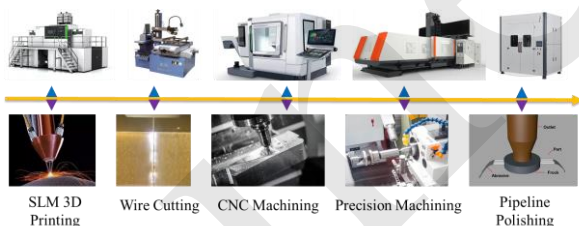

Fig. 10 Main equipment used in the manufacturing implementation

4 Hardware System

The WLR-IV single-legged robot developed by the design and manufacturing method proposed above is shown in Fig. 11. The robot contains three DOF of the hip pitch, knee, and driving wheel. The hip and knee are driven by the hydraulic drive unit (HDU) and the driving wheel is driven by a DC motor (TQ-ILM115 × 25). The HDU comprises a servo cylinder, a servo valve (star 200-0052), a displace-ment sensor (LVDT-70L), and two pressure sensors (HTS-25 Mpa), one for each of the two chambers of the cylinder. The motor driving the wheel is located at the calf near the knee joint. The motor drives the wheel through the helical gear (reduction ratio: 2.5) and synchronous belt (CEY896, reduction ratio: 2) two-stage deceleration transmission. The advantage of this design is that the moment of inertia of the shank is reduced. Since the impact force from the ground directly acts on the wheel, the synchronous belt can protect the motor from the impact. Moreover, the IMU sensor attached to the pelvis provides the posture information for balance control. A PC104 with a powerful CPU (Intel® Atom™ D525, 1.8 GHz) controller fixed on the pelvis is used to collect sensor information on the robot and control the HDUs and motor in real-time. The support bar limits the lateral tipping of the robot, but it is free in both the forward and vertical directions. In this way, WLR-IV single-legged robot can complete a jump motion freely.
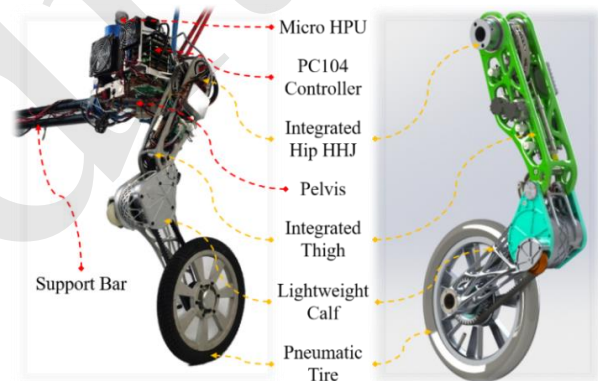

Fig. 11 WLR-IV single-legged robot experimental system

A micro HPU, which can output a maximum flow rate of 9 L/min under 21 MPa pressure, is also fixed to the pelvis. Its main function is to provide enough hydraulic power for the HDUs of the robot. A schematic diagram of the HPU is shown in Fig. 12a. The motor drives the pump to output high-pressure oil, which is directly transmitted to the HDUs through a one-way valve and high-pressure filter. An accumulator is installed on the high-pressure oil pipeline to eliminate pressure pulsation. After passing through the filter and cooler, the return oil from the HDUs is directly connected to the oil suction port of the pump. The accumulator on the low-pressure oil pipeline acts as an oil tank to compensate for the difference in volume of oil caused by the single-acting hydraulic

cylinder. There is a relief valve between the high-pressure and the low-pressure oil pipelines to set the overflow pressure. The information of temperature and pressure, motor speed and current, battery voltage and current is transmitted to the HPU servo controller, which outputs the control signal to the motor. Fig. 12b shows the structure and composition of the micro HPU. A customized external rotor motor is used to drive the plunger pump. The high-pressure oil from the pump passes through the micro accumulator and filter to obtain the hydraulic power required by the system.

An integrated hip HHJ (hydraulic hose-less joint (Li et al., 2019)) transfers the HPU's hydraulic power to the HDUs of the thigh and realizes the hose-less design of the robot. The thigh and pelvis are hinged through a deep groove ball bearing to realize the force transmission of the hip joint (Fig. 13). The sealing grooves for installing Glyd rings are designed in the central hole of the pelvis. The hydraulic power is transferred into the thigh through the hip oil router and the oil guiders. The hip
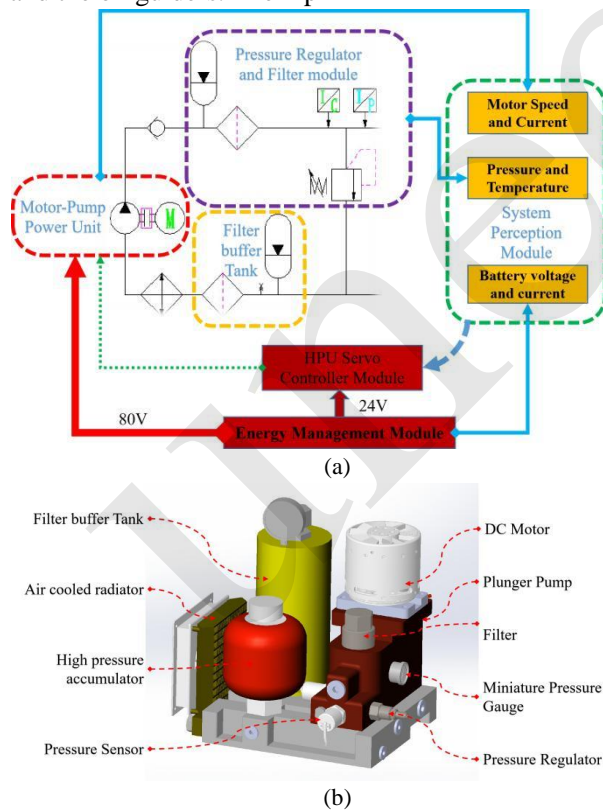
oil router is fixed to the thigh through two oil guiders, and rotates coaxially with the thigh in the central hole of the pelvis. The pelvic bone and hip oil router are integrated with the design and manufacturing method proposed in this paper, and the parallel oil circuit is integrated inside to increase the cross-sectional area of the oil circuit and improve heat dissipation efficiency.
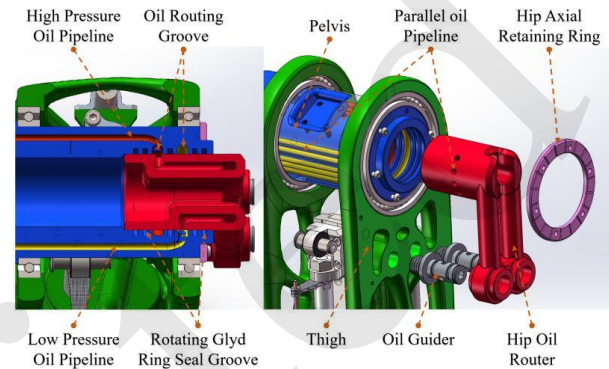

Fig. 13 The structural diagram of the hip HHJ

The torque, angle, and angular velocity parameters of each joint of the robot are listed in Table I. The joint torque is considered in the cylinder diameter and rod diameter design, and the range of joint rotation is considered in the cylinder stroke design. To obtain enough motion angle and angular velocity for each joint, the connecting rod size is adjusted to the appropriate length. The maximum torque of the joint is obtained from the product of the maximum load force of the hydraulic cylinder and the maximum moment arm length. The maximum load force of the cylinder is obtained under the rated pressure of 21 MPa. The maximum angular velocity is obtained from the maximum velocity of the cylinder.

Table 1 The joint range, angular velocity and driving torque of the WLR-IV single-legged robot.

Joint	RoM [rad]	Max. torque [Nm]@21 MPa	Max. angular velocity [rad/s]
Knee	0.61 – 3.11	240/91	28/68
Hip	-0.38 – 1.75	269/125	26/43

The mass and inertia of each link of the robot are presented in Table II. The pelvis contains the HPU (12 kg) and controller (3 kg).

(a)

(b)

Fig. 12 The schematic diagram(a) and composition structure(b) of the micro HPU

Table 2 Component parameters of the WLR-IV single-legged robot.

Name	Mass (kg)	Link Length (m)	Inertia (kg*m²)
Wheel	1.1	0.17	0.022
Shank	4.1	0.365	0.074
Thigh	3.3	0.351	0.032
Pelvis	23.2	0.066	0.206

4 Jump control

A wheel-legged robot is an inherently unstable system composed of a wheel and three rigid segments. To simplify the control strategy, the robot system was decoupled into a wheeled inverted pendulum model (WIPM) and a three-link model (Fig. 14), and corresponding controllers were designed to realize a vertical jump.

4.1 Balance control

Balance is the most fundamental of all motions of a wheel-legged robot. During the takeoff period, rapid movement of the multi-linkages will affect the balance of the robot system. Therefore, a proper balance controller is needed to make the robot more robust so that it can maintain balance during the jumping process.
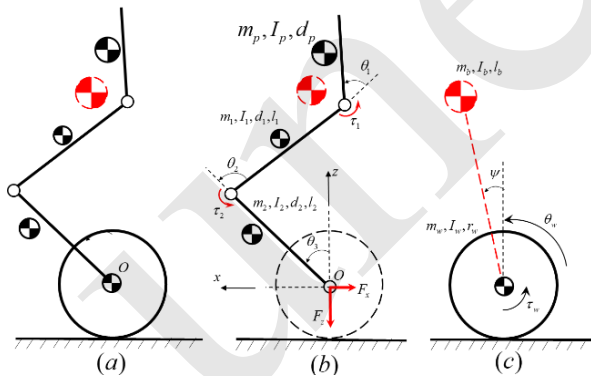

Fig. 14 The WLR-IV wheel-legged robot system (a) is decoupled into a wheeled inverted pendulum model (WIPM) (c) and a three-link model (b)

LQR was adopted in this study because of its mature calculation method and dynamic performance (Zhou et al., 2019). The choice of the state vector is $\boldsymbol{x}_{\text{w}} = [\psi\ \dot{\psi}\ \theta_{\text{w}}\ \dot{\theta}_{\text{w}}]^{\text{T}}$. The Euler-Lagrange based on the dynamic model of WIPM is linearized near the equi-

librium point and converted into the form of the state space equation, which can be written as

$$\dot{\boldsymbol{x}}_{\text{w}} = \boldsymbol{A}\boldsymbol{x}_{\text{w}} + \boldsymbol{B}\tau_{\text{w}} \qquad (1)$$

The quadratic performance index was chosen as $J = \int_0^\infty [\boldsymbol{x}_{\text{w}}^{\text{T}}\boldsymbol{Q}\boldsymbol{x}_{\text{w}} + R\tau_{\text{w}}^2]$, where $\boldsymbol{Q} \in \mathbf{R}^{4\times4}$ and $R \in \mathbf{R}$ are the weight matrix which determines the performance of the controller. By solving the Ricatti equation under different heights of the center of mass (COM), a series of feedback gains of the system are obtained. The relationship between feedback gains $\boldsymbol{K}$ and COM height l_{b} can be obtained by linear interpolation of these data. Then the wheel torque can be calculated by using the LQR control law:

$$\tau_{\text{w}} = -\boldsymbol{K}(l_{\text{b}}) \cdot \boldsymbol{x}_{\text{w}} \qquad (2)$$

4.2 Jump control strategy

Having designed a robust balance controller, multi-body movement is needed to complete the jump of the robot. One of the conditions of control strategy decoupling is to keep the COM of the robot above the center of the wheel, as the horizontal force of the multi-body on the wheel is always 0 to reduce the impact of a jump on the balance.

The dynamic model of the three-link structure in Fig. 12b is

$$\boldsymbol{M}(\boldsymbol{\theta})\ddot{\boldsymbol{\theta}} + \boldsymbol{C}(\boldsymbol{\theta},\dot{\boldsymbol{\theta}})\dot{\boldsymbol{\theta}} + \boldsymbol{G}(\boldsymbol{\theta}) = \boldsymbol{\tau} \qquad (3)$$

where $\boldsymbol{M}(\boldsymbol{\theta}) \in \mathbf{R}^{3\times3}$, $\boldsymbol{C}(\boldsymbol{\theta},\dot{\boldsymbol{\theta}}) \in \mathbf{R}^{3\times3}$ and $\boldsymbol{G}(\boldsymbol{\theta}) \in \mathbf{R}^3$ denote the inertia, Coriolis matrices, and gravity vector respectively. $\boldsymbol{\tau} = [\tau_1\ \tau_2\ 0]^T$ is the torque vector, and represents the torque applied on hip and knee joints. When $\psi \equiv 0$, the torque of the wheel $\tau_{\text{w}} \equiv 0$ according to the balance controller. Therefore, the ankle joint is an under-actuated joint, with a torque of 0.

Define the state variable $\boldsymbol{x} = [\boldsymbol{\theta}\ \dot{\boldsymbol{\theta}}]^{\text{T}}$, the dynamic Eq. (3) can be written in the following form:

$$\dot{\boldsymbol{x}} = \begin{bmatrix} \dot{\boldsymbol{\theta}} \\ -\boldsymbol{M}^{-1}(\boldsymbol{C}+\boldsymbol{G}) \end{bmatrix} + \begin{bmatrix} \mathbf{0} \\ \boldsymbol{M}^{-1}\boldsymbol{B} \end{bmatrix}\boldsymbol{\tau} \qquad (4)$$
$$= \boldsymbol{f}(\boldsymbol{x}) + \boldsymbol{g}(\boldsymbol{x})\boldsymbol{u}$$

Since the under-actuated system has two actuated joints, the following virtual constraints are introduced:

1) Keep the COM of the robot above the center of the wheel during the takeoff phase, s.t. $x_{com}(t) \equiv 0$.

2) Keep the knee joint tracking the desired trajectory.

System output can then be defined according to the virtual constraint

$$y = \begin{bmatrix} h_1(\boldsymbol{x},t) \\ h_2(\boldsymbol{x},t) \end{bmatrix} = \begin{bmatrix} x_{com}(t) - 0 \\ \theta_2(t) - \theta_{2d}(t) \end{bmatrix} \quad (5)$$

The balance controller for the WIPM can position the COM right above the wheels at the beginning of the takeoff period. Differentiate the output equation and keep the first and second-order differential at 0, through feedback linearization, the torques that can maintain the system on zero dynamic manifold $Z = \left\{ \boldsymbol{x} \middle| \boldsymbol{h}(\boldsymbol{x}) = L_f \boldsymbol{h}(\boldsymbol{x}) = \boldsymbol{0} \right\}$ can be obtained, and track the desired trajectory in the meantime (Berkemeier et al., 2019). The controller of the jump is:

$$\tau = -\frac{1}{L_g L_f \boldsymbol{h}} (L_f^2 \boldsymbol{h} + \boldsymbol{K}_p (\boldsymbol{x} - \boldsymbol{x}_d) + \boldsymbol{K}_d (\dot{\boldsymbol{x}} - \dot{\boldsymbol{x}}_d)) \quad (6)$$

The desired trajectory of the COM is determined by the expected jump height. The system is simplified as a one-dimensional SLIP model. According to the expected jump height, the velocity of the COM off the ground is obtained, and then the trajectory of the COM during the takeoff phase is obtained by solving the SLIP dynamic differential equation. The desired joint trajectory can be obtained by mapping the COM trajectory to joint space (Han et al., 2023).

The dynamic constraint of the robot in the flight phase is different from that in the standing phase (Goswami et al., 2009). In the flight phase, the relative position of the center of the wheel and the COM is controlled by adjusting the angle of the two actuated joints. The control trajectory of landing is the same as that for takeoff, which can be regarded as the reverse process of takeoff.

5 Experiments and results

In this section, an HDU displacement/force tracking and jump experiment is described that verifies the reliability of the structure and the effectiveness of the algorithm.

5.1 HDU displacement tracking

Displacement control is a necessary condition for the robot to accurately track the desired trajectory. To verify the displacement tracking performance of the HDU, a displacement tracking test was carried out, in which a simple proportional controller was adopted and the supply pressure was set at 12 Mpa. Firstly, the tracking performance of the step-up signal of the HDU displacement was tested. That is, the step signal tracking of the HDU when the piston rod is extended. The expected signal should step from 50 mm to 60 mm at 0.6 s. Fig. 15 shows that the HDU of the knee joint tracked the step-up signal in 0.2 s. Then the step-down signal tracking of piston rod was tested. The experimental results are shown in Fig. 16. The down-step signal tracking time was equivalent to the step-up time, which shows that the simple P controller can achieve the control target well. The steady-state error of the step was close to 0, which also indicates that HDU has a good displacement tracking performance. Finally, to test the tracking performance of sinusoidal signals, the instruction of the knee cylinder was expected to be a sinusoidal displacement with an intermediate value of 40 mm and an amplitude of 5 mm at a frequency of 2 Hz. Experimental results in Fig. 17 show that the HDU of the knee could track the expected displacement command well. The above displacement step and sinusoidal tracking tests showed the good HDU tracking performance of the WLR-IV single-legged robot, and established the foundation for the following experiments. In subsequent experiments, feed-forward control was added and PID control parameters optimized to improve displacement tracking performance.
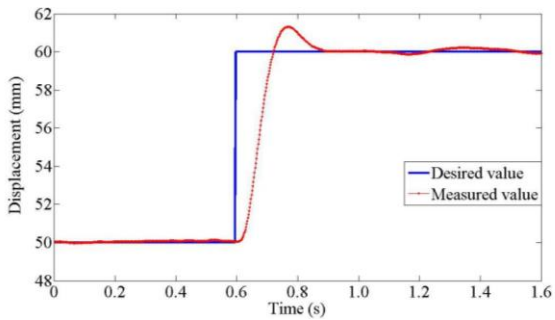
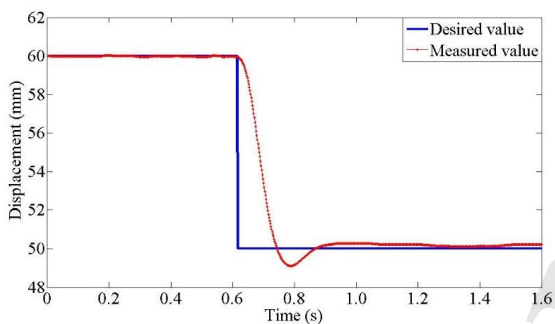**Fig. 15 The knee HDU displacement step-up tracking performance**

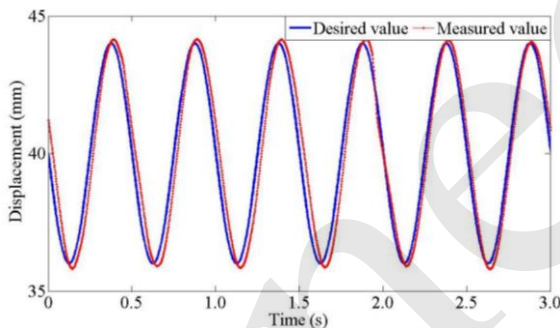**Fig. 16 The knee HDU displacement step-down tracking performance**

Fig. 17 The knee HDU displacement sinusoidal signal tracking performance

5.2 HDU force tracking

Accurate and fast force tracking performance is needed for the robot to achieve compliance control. In the force tracking experiment, we adopted a simple proportional controller. In this test, the supply pressure was 12 Mpa and the wheel maintained contact with the ground. Firstly, the step tracking performance of the knee joint HDU was tested, including step-up and step-down signal tracking. The expected signal of the step-up increased from 2500 N to 3000 N while the step-down decreased from 3000 N to 2500 N.
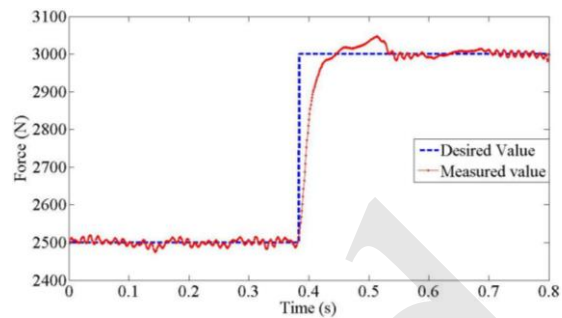
Fig. 18 The knee HDU force step-up tracking performance

The experimental results of step-up and step-down are shown in Fig. 18 and Fig. 19 respectively. The actual force of the HDU tracked the expected signal within 0.1 s and maintained a steady-state error of less than 1%. Fig. 20 presents the experimental result of sinusoidal force tracking of the knee HDU. The median of the sinusoidal expected force for the knee joint was 2500 N, and the amplitude was 500 N with a frequency of 2 Hz. The sinusoidal force tracking results showed that the HDU had good force tracking performance, which provides a guarantee for the jump control of the wheel-legged robot based on force control.
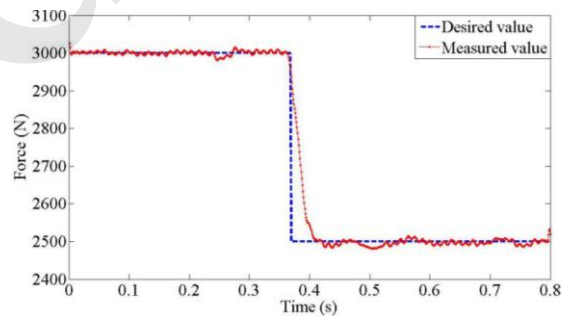

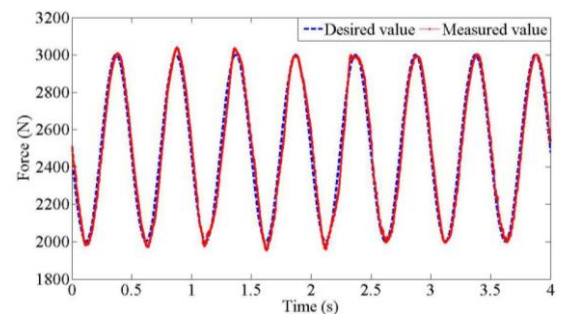**Fig. 19 The knee HDU force step-down tracking performance**

Fig. 20 The knee HDU force sinusoidal signal tracking performance

5.3 Jump experiment

Jumping requires a strong explosive force and a reliable structure. The jump of the WLR-IV single-legged robot not only reflects its strong driving ability but also verifies the effectiveness of the design method proposed in Section 2 and the manufacturing method proposed in Section 3. It also proves the effectiveness of the balance control strategy and jump planning method proposed in Section 5. Fig. 21 shows the jump process of the WLR-IV single-legged robot. When the robot is ready to jump, the hydraulic power unit increases the output pressure of the system by more than 17 Mpa. Then the central controller controls the hydraulic drive units of the knee joint and hip joint to follow the planned jumping trajectory. When the robot is in the flight phase, the hydraulic power unit reduces the output pressure to 10 MPa to prepare for the landing buffer. Fig. 22 and Fig. 23 show the knee and hip angle tracking during the jump. The knee HDU needs high power output with high speed and high torque, so the tracking performance of the knee HDU is not as good as that of the hip HDU. The joint torque during the jumping process in Fig. 24 shows that the knee joint output torque is larger than that of the hip joint. Especially when landing, the knee joint peak torque reaches 260 Nm. Under such a large impact force, the structure of the WLR-IV single-legged robot withstood the test.
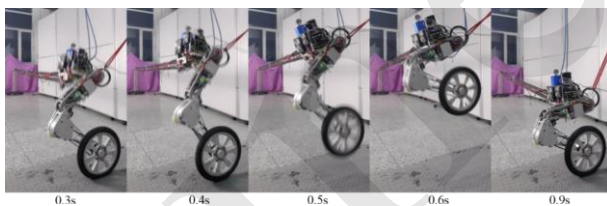

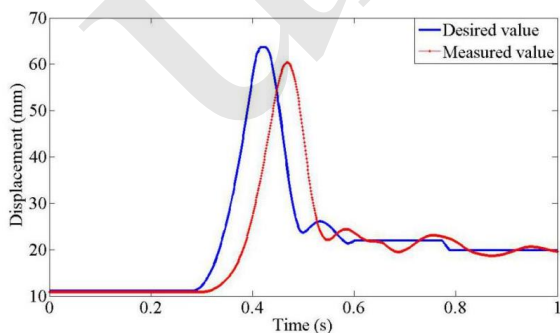**Fig. 21 Snapshots from the jump experiment**

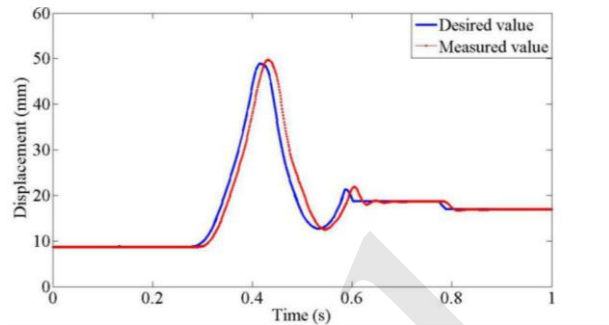**Fig. 22 The knee HDU displacement tracking performance**

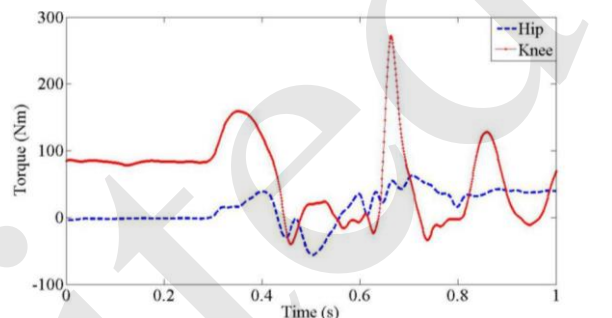**Fig. 23 The hip HDU displacement tracking performance**

Fig. 24 The hip and knee joint torque

Fig. 25 shows the change in height of the COM of the WLR-IV single-legged robot. The jumping height of the robot is close to 0.6 m. Fig. 19 shows that the height of the wheel above the ground was more than 0.45 m. The robot jump experiment was repeated several times and there was no damage to the structure of the robot, which fully verifies the reliability of the structure and the effectiveness of the design and manufacturing method.
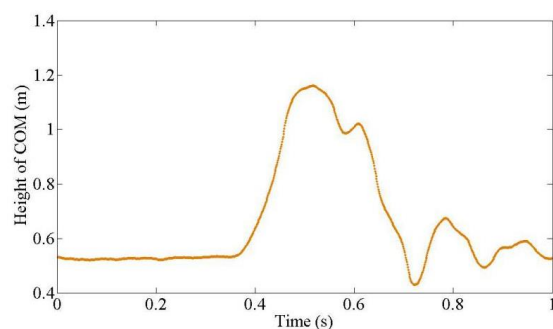

Fig. 25 The change in height of the COM

6 Conclusions

This paper presents a lightweight design and integrated manufacturing (LD&IM) methodology tailored for hydraulic wheel-legged robots. By leveraging topology optimization and generative

design techniques, we introduce a novel lightweight design method that has been successfully implemented in the creation of the WLR-IV single-legged robot, significantly reducing its weight to 7.5 kg, compared to the 13.7 kg of the WLR-II's leg. Bridging the gap between CAD models and real-world components, we propose an integrated manufacturing approach, combining precision machining with additive manufacturing (AM). This research offers a valuable framework for the design and production of hydraulic-driven robots.

Furthermore, we demonstrated the effectiveness of our approach by implementing a balance controller based on a linear quadratic regulator (LQR) and a jump trajectory planner based on a spring-loaded inverted pendulum (SLIP) model in the WLR-IV single-legged robot, enabling it to achieve a 0.45-m-high jump. These successful experimental outcomes not only represent a technical milestone but also provide a methodological blueprint for researchers grappling with the challenges of constructing high-performance and highly integrated hydraulic driven robots. As far as our knowledge extends, this is the first comprehensive exploration of these topics.

While 3D printing or AM offers clear advantages in terms of light weight and strength, the intricate design, complex manufacturing processes, and elevated costs are primary hurdles inhibiting mass production of repetitive components. Particularly for hydraulic-driven robots, in which complex components impose stringent demands for light weight and high-strength structures, the integration of hydraulic drive units, diverse sensors, accumulators, heat dissipation structures, and other functional elements into the framework necessitates precision machining processes that can meet exacting tolerance standards. In the future, the synergy between AM and traditional subtractive manufacturing (SM), along with advancements in material production technology, will steer the evolution of intelligent lightweight structures with heightened stiffness and strength. Additionally, enhancing the automation and intelligence of design and manufacturing processes will be a focal point for our ongoing research.

Acknowledgments

Author contributions

X.L. designed the research. H.Y. and H. Z. processed the corresponding data. X.L. wrote the first draft of the manuscript. H. Y. and H.F. helped to organize the manuscript. H.F. revised and edited the final version. X.L. and Y.F. provided funding support.

Conflict of interest

The authors declare that they have no known competing financial interests or personal relationships that could have appeared to influence the work reported in this paper.

References

Bae H, Lee I, Jung T, et al., 2016. Walking-wheeling dual mode strategy for humanoid robot, DRC-HUBO+. IEEE/RSJ International Conference on Intelligent Robots and Systems (IROS), p.1342-1348.

Berkemeier MD, Fearing RS, 1999. Tracking fast inverted trajectories of the underactuated acrobot. *IEEE Transactions on Robotics and Automation*, 15(4):740-750.

Brice C, Shenoy R, Kral M, et al., 2015. Precipitation behavior of aluminum alloy 2139 fabricated using additive manufacturing. *Materials Science Engineering: A*, 648: 9-14.

DeDonato M, Polido F, Knoedler K, et al., 2017. Team WPI-CMU: achieving reliable humanoid behavior in the DARPA robotics challenge. *Journal of Field Robotics*, 34(2): 381-399

Emmelmann C, Kranz J, Herzog D, et al., 2014. Laser additive manufacturing of metals. Laser technology in biomimetics: basics and applications. Berlin, Heidelberg: Springer Berlin Heidelberg, p.143-162.

Glowinski S, Krzyzynski T, Bryndal A, et al., 2020. A kinematic model of a humanoid lower limb exoskeleton with hydraulic actuators. *Sensors*, 20(21): 6116.

Goswami D, Vadakkepat P, 2009. Planar bipedal jumping gaits with stable landing. *IEEE Transactions on Robotics*, 25 (5): 1030-1046.

Großmann A, Weis P, Clemen C, et al., 2020. Optimization and re-design of a metallic riveting tool for additive manufacturing—A case study. *Additive Manufacturing*, 31: 100892

Han Y, Liu G, Lu Z, et al., 2023. A stability locomotion-control strategy for quadruped robots with center-of-mass dynamic planning. *Zhejiang Univ. Sci. A* 24, 516–530. https://doi.org/10.1631/jzus.A2200310

Herzog D, Seyda V, Wycisk E, et al., 2016. Additive manufacturing of metals. *Acta Materialia*, 117: 371-392.

Hyon SH, Suewaka D, Torii Y, et al., 2016. Design and experimental evaluation of a fast torque-controlled hydrau-

lic humanoid robot. *IEEE/ASME Transactions on Mechatronics*, 22(2): 623-634.

Karumanchi S, Edelberg K, Baldwin I, et al., 2017. Team RoboSimian: semi-autonomous mobile manipulation at the 2015 DARPA robotics challenge finals. *Journal of Field Robotics*, 34 (2): 305-332.

Kien D and Zhuang X, 2021. A deep neural network-based algorithm for solving structural optimization. *Journal of Zhejiang University Science A,* 22(8): 609-620.

Klemm V, Morra A, Salzmann C, et al. 2019. Ascento: a two-wheeled jumping robot. In 2019 International Conference on Robotics and Automation (ICRA). IEEE, 2019: 7515-7521.

Knabe C, Griffin R, Burton J, et al., 2018. Team VALOR's ESCHER: a novel electromechanical biped for the DARPA robotics challenge. *The DARPA Robotics Challenge Finals: Humanoid Robots to The Rescue. Springer, Cham*, p.583-629.

Krish S, 2011. A practical generative design method. *Computer-Aided Design*, 43(1), 88-100.

Li X, Feng HB, Zhang SY, et al., 2019. Vertical Jump Control of Hydraulic Single Legged Robot (HSLR). IEEE/ASME International Conference on Advanced Intelligent Mechatronics (AIM), p.1421-1427.

Li X, Zhou HT, Feng HB, et al., 2018. Design and Experiments of a Novel Hydraulic Wheel-legged Robot (WLR). IEEE/RSJ International Conference on Intelligent Robots and Systems (IROS), p.3292-3297.

Li X, Zhou HT, Zhang SY, et al., 2019. WLR-II, a Hose-less Hydraulic Wheel-legged Robot. IEEE/RSJ International Conference on Intelligent Robots and Systems (IROS), p.4339-4346.

Liu J, Gaynor AT, Chen S, et al., 2018. Current and future trends in topology optimization for additive manufacturing. *Structural and multidisciplinary optimization*, 57(6): 2457-2483.

Maddikunta, P. K. R., Pham, Q. V., Prabadevi, B., Deepa, N., Dev, K., Gadekallu, T. R., ... & Liyanage, M., 2022. Industry 5.0: A survey on enabling technologies and potential applications. *Journal of Industrial Information Integration, 26, 100257.*

Maher ML, Poon J, 1996. Modeling design exploration as co-evolution. *Computer-Aided Civil and Infrastructure Engineering*, 11 (3): 195-209.

Majern k, M., Daneshjo, N., Malega, P., Dr bik, P., & Barilov á B., 2022. Sustainable development of the intelligent industry from Industry 4.0 to Industry 5.0. *Advances in Science and Technology. Research Journal, 16(2), 12-18.*

Martin JH, Yahata BD, Hundley JM, et al., 2017. 3D printing of high-strength aluminium alloys. *Nature*, 549 (7672): 365-369.

Ngo TD, Kashani A, Imbalzano G, et al., 2018. Additive manufacturing (3D printing): A review of materials, methods, applications and challenges. *Composites Part B: Engineering*, 143: 172-196.

Raibert M, Blankespoor K, Nelson G, et al., 2008. Bigdog, the rough-terrain quadruped robot. *IFAC Proceedings Volumes*, 41(2): 10822-10825.

Rong XW, Li YB, Ruan J, et al., 2012. Design and simulation for a hydraulic actuated quadruped robot. *Journal of mechanical science and technology*, 26(4): 1171-1177

Semini C, Barasuol V, Goldsmith J, et al., 2016. Design of the hydraulically actuated, torque-controlled quadruped robot HyQ2Max. *IEEE/ASME Transactions on Mechatronics*, 22 (2): 635-646.

Semini C, Goldsmith J, Manfredi D, et al., 2015. Additive manufacturing for agile legged robots with hydraulic actuation. International Conference on Advanced Robotics (ICAR), p.123-129.

Stentz A, Herman H, Kelly A, et al., 2016. CHIMP, the CMU highly intelligent mobile platform. *Journal of Field Robotics*, 32 (2): 209-228.

Sun, Y., Zong, C., Pancheri, F., Chen, T., & Lueth, T. C., 2023. Design of topology optimized compliant legs for bio-inspired quadruped robots. Scientific Reports, 13(1): 4875.

Tsagarakis NG, Caldwell DG, Negrello F, et al., 2017. Walkman: A high‐performance humanoid platform for realistic environments. *Journal of Field Robotics*, 34(7): 1225-1259.

Wu J, Qian X, Wang MY, 2019. Advances in generative design. *Computer Aided Design*, 116: 102733.

Yap, CY, Chua, CK, Dong, ZL, et al., 2015. Review of selective laser melting: Materials and applications. *Applied physics reviews*, 2(4):041101.

Zhang J, Huang H, Liu G, et al., 2021. Stiffness and energy absorption of additive manufactured hybrid lattice structures. *Virtual and Physical Prototyping*, 16(4): 428-443.

Zhou HT, Li X, Feng HB, et al., 2019. Model Decoupling and Control of the Wheeled Humanoid Robot Moving in Sagittal Plane. IEEE-RAS 19th International Conference on Humanoid Robots (Humanoids), p.1-6.

Zhou M, Rozvany G,1991. The COC algorithm, part II: topological, geometrical and generalized shape optimization. *Computer Methods in Applied Mechanics and Engineering*, 89(1–3):309–336.

Electronic supplementary materials
Section S1

中文概要

题 目：液压轮腿机器人的轻量化设计与一体化制造方法

作 者： 李旭 [1,2]，于淏阳 [1]，纵怀志 [2]，封海波 [1]，付宜利 [1]

机 构： [1] 哈尔滨工业大学，机器人技术与系统国家重点实验室，中国哈尔滨，150001；[2] 浙江大学，流

体动力与机电系统国家重点实验室，中国杭州，310027

目　　的： 设计和制造方法对液压驱动机器人的研制至关重要。本文将建立液压轮腿机器人从概念模型到实际机器人的完整研制过程，所提出的轻量化设计与一体成型制造（LD&IM）方法使机器人研制过程更加高效，实现45%减重目标和45cm竖直跳跃。

创新点： 1. 提出了基于拓扑优化与衍生设计的液压轮腿机器人的轻量化设计方法和基于3D打印的一体成型制造方法；2. 提出了一种基于LQR的轮腿机器人跳跃控制方法。

方　　法： 1. 采用基于拓扑优化和衍生设计的强量化设计方法，实现了轮腿机器人结构45%的减重目标；2. 结合选择性激光熔化工艺和相应的高精度抛光的一体成型制造工艺，可以快速高效地完成高质量零件的一体成形；3. 在单轮腿机器人的平衡控制回路中使用了线性二次型调节器（LQR）和基于零动态的控制器，将弹簧负载倒立摆（SLIP）模型应用于机器人跳跃运动的轨迹规划。

结　　论： 1. 采用基于拓扑优化与衍生设计的液压轮腿机器人轻量化设计方法实现了45%的减重目标；2. 精密加工与3D打印相结合的一体成型制造方法使机器人研制过程更加高效；3. 基于LQR的平衡控制器和基于SLIP的跳跃轨迹规划器应用于WLR-IV单腿，实现了0.45米竖直跳跃。

关键词： 轮腿机器人；液压驱动；拓扑优化；增材制造；跳跃控制